# Chapter 10
# A Temporally Varied Rainfall Simulator for Flash Flood Studies


**Mohammad Ebrahim Banihabib and Bahman Vaziri**

**Abstract** Experimental studies of flash floods require rainfall simulations. For this reason, various rainfall simulators have been designed, built, and employed in previous studies. These previous rainfall simulators have provided good simulations of constant rainfall intensities; however, these simulators cannot generate temporally varied rainstorms. Thus, the effect of the temporal distribution of a rainstorm on flash flooding cannot be studied using current rainfall simulators. To achieve accurate and reliable results in flash flood studies, simulating rainstorms that are similar to natural precipitation events is essential, and natural rainfall varies temporally. Thus, a rainstorm simulator was designed and built using cascading tanks to generate rainstorm hyetographs that cannot be obtained using traditional rainfall simulators. The result of the rainstorm generated by the proposed instrument and its numerical model showed that the instrument can simulate the temporal distributions of rainstorms with an accuracy of 95 percent. Consequently, the proposed instrument and its numerical model can be applied for generating artificial rainstorm hyetographs in experimental and field studies of flash floods.

**Keywords** Rainfall simulator · Rainfall hyetograph · Cascade reservoir routing · Rainfall temporal distribution flash flood

M. E. Banihabib (✉)
Department of Water Engineering, Aburaihan Campus, University of Tehran, Tehran, Iran
e-mail: banihabib@ut.ac.ir

B. Vaziri
Water Resources Engineering, Department of Water Engineering, Aburaihan Campus, University of Tehran, Tehran, Iran
e-mail: b.vaziri@ut.ac.ir



T. Sumi et al. (eds.), *Wadi Flash Floods*, Natural Disaster Science and Mitigation Engineering: DPRI Reports, https://doi.org/10.1007/978-981-16-2904-4_10

## 10.1 Introduction

Flash floods are frequently reported in arid and semiarid regions in Iran, Iraq, Egypt, and Oman (Al-Rawas and Valeo 2009; Banihabib and Tanhapour 2020; de Vries et al. 2013; Mustafa et al. 2019). For example, debris floods are flash floods that occur in the mountainous areas of Mazandaran and Golestan Provinces, Iran (Banihabib and Tanhapour 2020). Flash floods were also reported in various provinces in Iran during the period from 1962 to 2002 (Tabari and Willems 2016). In this period, the total flood damage was appraised to be US$138 million. Roughani et al. (2007) reported that heavy rainfall was a key factor in the flash floods that occurred in this period. Recently, in March–April 2019, widespread flash floods damaged most provinces of Iran, causing over $3.5 billion U.S. dollars in destruction (Aminyavari et al. 2019).

Flash floods are triggered by highly intense rainstorms in arid and semiarid areas, and flood hyetographs typically display fast growth, even for large catchments. Thus, the temporal characteristics of rainstorms are the main characteristics used to study the temporal distributions of flash floods (Mays 2001). For example, even though major dissimilarities between the rainstorm depths of the coastal and mountainous zones were reported, a strong consistency in only the temporal distributions of rainstorms that caused flash floods in Oman was observed (Al-Rawas and Valeo 2009). In another study, Mustafa et al. (2019) showed that the intensity rates and temporal distributions of rainstorms are among the key features of flash floods in Iraq's north region.

Rainfall simulators are useful devices for generating artificial rain, and they are used in various rainfall-runoff and soil erosion studies. In addition, data obtained from studies that use these devices can be employed for the verification, calibration, and evaluation of soil erosion and flash flood prediction models (Sangüesa et al. 2010). Therefore, rainfall simulators are widely used as a useful instrument in flash flood field experiments. To date, these devices have been widely employed in various studies to determine soil erosion, runoff, and rainfall percolation in soil (Esteves et al. 2000; Fernández-Gálvez et al. 2008; Foster et al. 2000; Grierson and Oades 1977; Moore et al. 1983).

Aoki and Sereno (2006) employed a small rainfall simulator to study the infiltration of water into the earth in a 0.0625 $m^2$ square plot. The height of this rainstorm simulator was 1.5 m, and the required pressure to form raindrops was provided by a water tank. Cornelis et al. (2004) used a wind tunnel and a rainstorm simulator to study the effects of wind and rainstorm characteristics on the amount of soil erosion. In their research, the employed rainstorm simulator had sprinklers that were able to simulate precipitation with different constant intensities using a pressurized water system. Simulations of rainfall by these devices are often performed using one of two different methods: nozzle rainfall simulations and drop-forming simulations (Corona et al. 2013). In the first method, the simulation of rainstorms is performed by the use of water distribution nozzles. In this method, pressurized nozzles are embedded in the device, allowing the adjustment of the

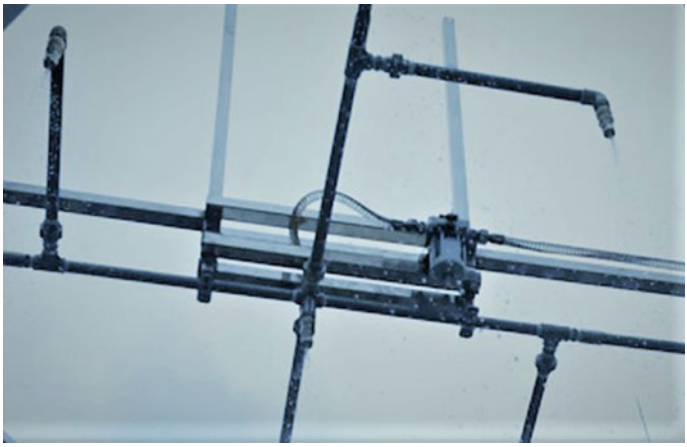

**Fig. 10.1** A nozzle rainstorm simulator

simulated rainstorm intensity based on the water pressure in the system. A device of this type is shown in Fig. 10.1.

In the second type, artificial raindrops fall using gravity from holes installed in the device. Generally, the simulated precipitation intensity of these instruments is adjusted by a device known as a Mariotte bottle. A device of this type is shown in Fig. 10.2. This kind of simulator consists of two main parts, a Mariotte bottle for adjusting the amount of water that is let out and the water drainage holes (Huang et al. 2013). The Mariotte bottle is a device used for adjusting a constant rate of flow from a cylindrical or cubic tank and a pipe through which air enters the tank with vertical movement inside the bottle. The amount of air entering the bottle can be adjusted, which leads to the adjustment of the rainfall rate out of the bottle.

Although these simulation technologies can satisfactorily simulate rainfall of a certain intensity, they are not capable of making rainfall hyetographs (temporal variations in rainfall). Under natural conditions, the intensity of rainfall during a storm period is not constant, and rainstorms always start with low intensity. After a while the precipitation reaches its peak; then, the intensity decreases, and finally, the rainstorm stops. Ensuring the accuracy and similarity of simulated rainfall events to the temporal distributions of actual rainfall events is crucial for obtaining precise and reliable results in flash flood and soil erosion studies. Therefore, the invention of new methods for simulating the temporal distributions of rainstorms is necessary. Accordingly, the main purpose of this research is to design and examine a rainfall generator to produce various rainfall hyetographs for a more accurate examination of the different temporal distributions of rainstorms in flash flood studies.

**Fig. 10.2** A constant rainstorm simulator

## 10.2 Material and Methods

The main disadvantage of existing rainfall simulators is that they can only generate a constant rainfall intensity. By designing and constructing hyetograph-generating devices, as shown in Fig. 10.3, the proposed rainfall simulator can simulate temporally varied precipitation using drop-forming simulator technology and a cascading tank model. The cascading tank model has previously been used by some researchers for flood simulations [8], and in this research, the model was developed for temporally varied rainstorm simulations. The hyetograph-generating device is made up of two main parts, including two tanks: one for water retention and another tank for rainfall generation. The outflow can be adjusted by a valve in the first tank outlet which controls the rising limb of the generated rainfall hyetograph, and the drop holes in the second tank produce and control the receding limb of the generated rainfall hyetograph. At the end of the valve, a shower head is installed to prevent turbulence in the water surface of the second tank. At the bottom of the second tank, there are 50 holes, each with a diameter of 1 mm. The simulated rainfall intensity is a function of the area of these holes and the water head in the tank. The discharge of water from these holes can be adjusted by changing the area of the outlet holes to simulate precipitation with varying intensities. Additionally, to adjust the precipitation intensity, the diameter of the outlet holes can be adjusted by inserting plastic threads of different thicknesses in these holes.

To simulate specific precipitation with the device, reservoir flood routing is required in the tanks. The output discharge from the tanks can be obtained from Eq. (10.1) (Almutairi and Zribi 2006):

$$Q_t = CA\sqrt{2gh_t} \tag{10.1}$$

**Fig. 10.3** The rainstorm hyetograph-generating device

where $Q_t$ is the flow discharge from the tank at time $t$, $C$ is the orifice coefficient, $A$ is the orifice area, $g$ is the gravitational acceleration and $h_t$ is the water head in the tank at time $t$. Further, according to the definition of discharge, the outflow from the tank is equivalent to the water storage variation in the tank in a given time increment and can thus be expressed in terms of the water depth variation, as presented in Eq. (10.2):

$$Q_t = \frac{\mathrm{d}V}{\mathrm{d}t} = \pi r^2 \frac{\mathrm{d}h}{\mathrm{d}t} \tag{10.2}$$

where $V$ is the water volume in the tank, $r$ is the tank radius, $h$ is the height of the water in the tank and $t$ is time.

Since the walls of the tank used in the device have a small slope, the radius value in Eq. (10.2) at moment $t$ is a function of the value of $h$ and can be calculated according to Eq. (10.3):

$$r = R1 + \frac{R2 - R1}{H} h_t \tag{10.3}$$

where $r$ is the tank radius at time $t$, $R1$ is the radius of the tank bottom, $R2$ is the radius of the tank surface at the highest point and $H$ is the height of the tank. By replacing Eqs. (10.1) and (10.3) in Eq. (10.2), we obtain Eq. (10.4) as follows:

$$CA\sqrt{2gh_t} = \pi\left(R1 + \frac{R2 - R1}{H}h_t\right)^2\frac{\Delta h}{\Delta t} \tag{10.4}$$

By measuring the variations in the water head in the tank at specified intervals, it is possible to determine the value of $C$ by calibration in Eq. (10.4). Additionally, to measure the error indexes of the model calibration and validation, the mean absolute relative error (MARE) was used, as shown in Eq. (10.5):

$$\text{MARE} = \frac{\sum_{i=1}^{n}|X_o - X_c|/X_o}{n} \tag{10.5}$$

where $X_O$ is the value of the observed water depth, $X_C$ is the value of the calculated water depth and $n$ is the number of measured water depths. Thus, by determining the water head value in the tank, it is possible to calculate the amount of water outflow from the tanks using Eq. (10.1) and thus calculate the rainstorm intensity and eventually define a simulated rainfall hyetograph. Therefore, the device can be adjusted to generate various rainfall hyetographs.

## 10.3 Results and Discussion

In this study, the calibration of the device was carried out only with a fully open valve in the first tank and with a hole diameter of 1 mm. The generated hyetograph was obtained under these circumstances. However, depending on the needs of the researcher, it is possible to similarly calibrate and produce different hyetographs. For this purpose, the values of the water heads were recorded in both tanks at a time interval of 30 s. Since the value of parameter $C$ is not constant and is a function of the water head in the tank, the best equation was obtained for estimating the value of parameter $C$ for each tank using regression analysis. Equations (10.6) and (10.7) were derived for the first and second tanks using regression analysis, respectively. As shown in Eqs. (10.6) and (10.7), the value of $C$ is a function of the ratio of the water head to the diameter of the hole. Equations (10.6) and (10.7) are expressed as follows:

$$C_1 = 1.3\left(\frac{h_1}{D_1}\right)^{-0.275} \tag{10.6}$$

$$C_2 = 2.3\left(\frac{h_2}{D_2}\right)^{-0.25} \tag{10.7}$$

where $C_1$ and $C_2$ are the orifice coefficients in the first and second tanks, respectively; $h_1$ and $h_2$ are the water heads in the first and second tanks, respectively; $D_1$ is the diameter of the water outlet orifice in the first tank; and $D_2$ is the equivalent diameter of the holes in the second tank.

In the next step, based on the values obtained for the parameters $C_1$ and $C_2$ from Eqs. (10.6) and (10.7), the values of the parameter $h$ were calculated using Eq. (10.4) for each tank and compared with the observed values of $h$. The results are shown in Figs. 10.4, 10.5, 10.6 and 10.7.

In Fig. 10.4, the values of the observation water heads and those calculated Eq. (10.4) are displayed over time for the first tank. The value of $C_1$ is calculated using Eq. (10.6). As shown, the calculated water head values for the first tank at the beginning of the graph have acceptable agreement with the observed data, and this trend continues up to 250 s. After this time, there is a difference between the observed and calculated values in the middle of the chart; however, these values approach each other again, and the calculated water head values agree with the observed values. Additionally, in Fig. 10.5, the calculated water head values versus the observed values are displayed on the vertical and horizontal axes, respectively. As shown in Fig. 10.5, the data are generally close to a perfect line, and there are only some differences between the observed and calculated data in the middle and the end of the graph. This indicates that the high water head values calculated using Eq. (10.4) are a good estimation relative to the observed water head values. The differences between the calculated and observed values in the middle and the end regions of both plots can be attributed to errors in measuring the water levels in the tanks. The exact magnitudes of these errors were calculated using Eq. (10.5), and according to the observed data, the average error was 4.5% for the first tank. Therefore, the simulated water head values can be used to estimate the actual water head values in the first tank of the device with acceptable accuracy.

Figures 10.6 and 10.7 are the same as Figs. 10.4 and 10.5 but display values for the second tank; the observed water head values and the values calculated using

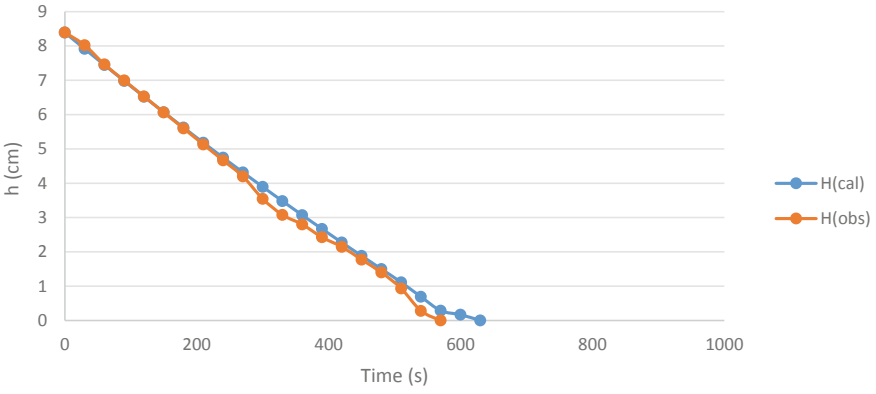


**Fig. 10.4** The observed and calculated water head values versus time in the first tank

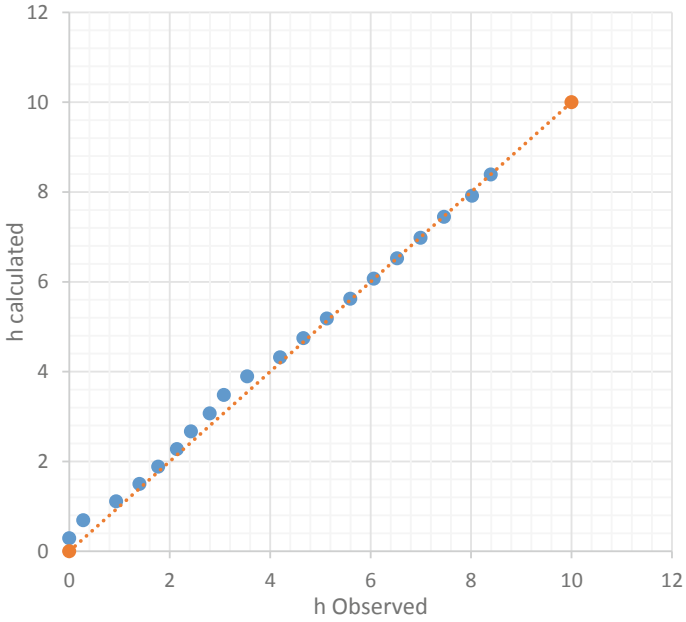


**Fig. 10.5** The observed water head values versus the calculated water head values in the first tank

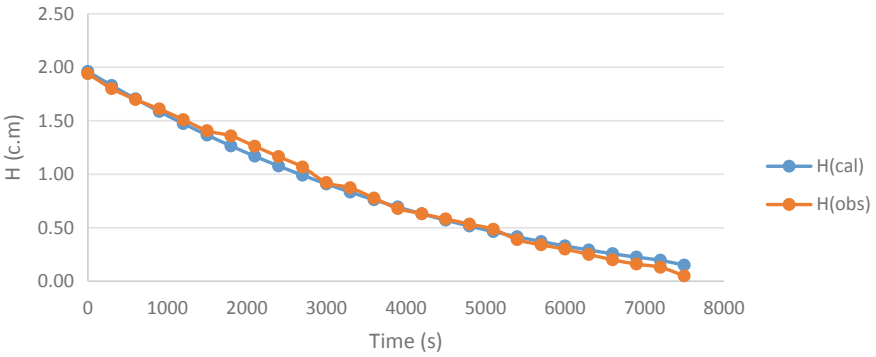


**Fig. 10.6** The observed and calculated water head values versus time in the second tank

Eq. (10.4) based on the values of the $C_2$ parameters for the second tank are displayed over time. As shown in Fig. 10.6, the calculated water head values agreed well with the observed values, except for those in the middle and the end of the diagram. In addition, in Fig. 10.7, the calculated versus observed water head values are similar to a perfect line except for at the beginning and the end of the chart. As previously stated, the differences between the calculated and observed values in the divergent parts of both charts can be attributed to errors in measuring the water

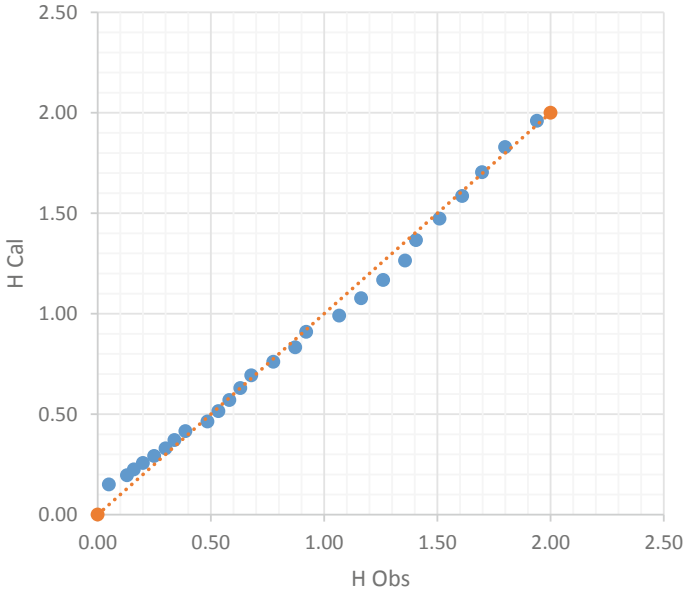


**Fig. 10.7** The observed water head values versus the calculated water head values in the second tank

levels in the tank. The error calculated from Eq. (10.5) is equal to 4.9% for the second tank. Therefore, as shown in Figs. 10.6 and 10.7 as well as the calculated error rate, the calculated water head values represent acceptable estimations with good accuracy for the simulation of the water heads in the second tank.

By calculating $C_1$ and $C_2$ using Eqs. (10.6) and (10.7) for each tank and replacing these values in Eq. (10.4), it is possible to estimate the water head value in each tank, and accordingly, the different rainstorm hyetographs can be estimated for various initial water heads in the first tank. To show the rainstorm hyetograph of the device, a water level of 9 cm in the first tank was considered as the initial head value. Using this head, the water levels in the tanks were calculated from Eq. (10.4) within a 30-s time interval, and finally, the rainstorm hyetograph was simulated. Figures 10.8, 10.9 and 10.10 show the trends of the water head changes in the first and second tanks and the rainstorm hyetographs, respectively.

Figure 10.8 shows the water head variation in the first tank over time. As shown in this chart, the water head in the first tank begins to drop from the initial head (9 cm) and continues to drop with a constant gradient. Finally, the water volume of the first tank is totally discharged into the second tank after nearly 700 s. This flow time, as shown in Figs. 10.9 and 10.10, directly affects the time it takes to reach the peak in the output hyetograph and the peak flow time of the flash floods in the experiments. When water is discharged from the first tank, the water head in the second tank gradually rises. Finally, as the first tank completely empties, the water head reaches its maximum in the second tank. Since the discharge from the holes is

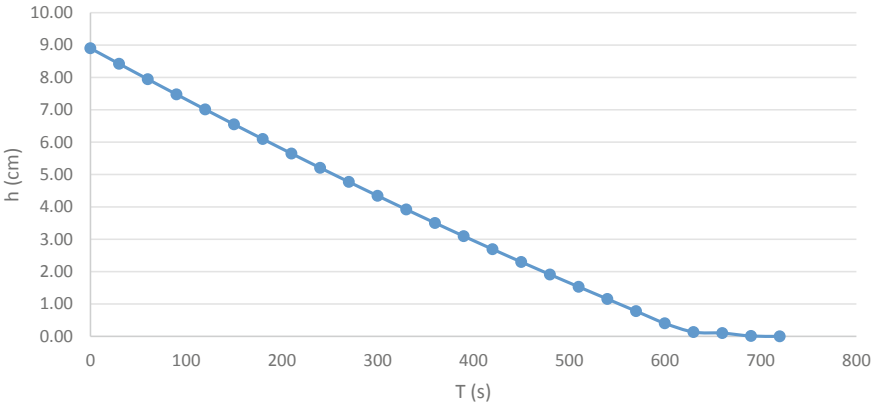


**Fig. 10.8** The water head changes in the first tank

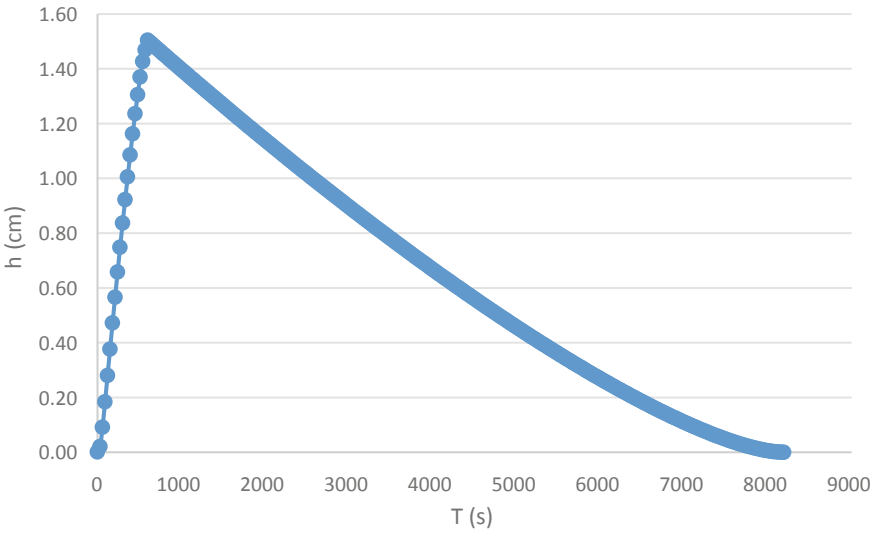


**Fig. 10.9** The water head changes in the second tank over time

a function of this second-tank water head according to Eq. (10.1), by reaching the maximum water head value in the second tank, the water outflow from the second tank of the device (rainstorm intensity) reaches its maximum. Therefore, the highest rainstorm intensity is observed at this point. Moreover, it can be concluded that the duration of water discharging from the first tank directly affects the shape of the rainstorm hyetograph, and thus, with the adjustment of the valve installed on the outlet of the first tank, it is possible to create different rainstorm hyetographs with different times to the peaks.

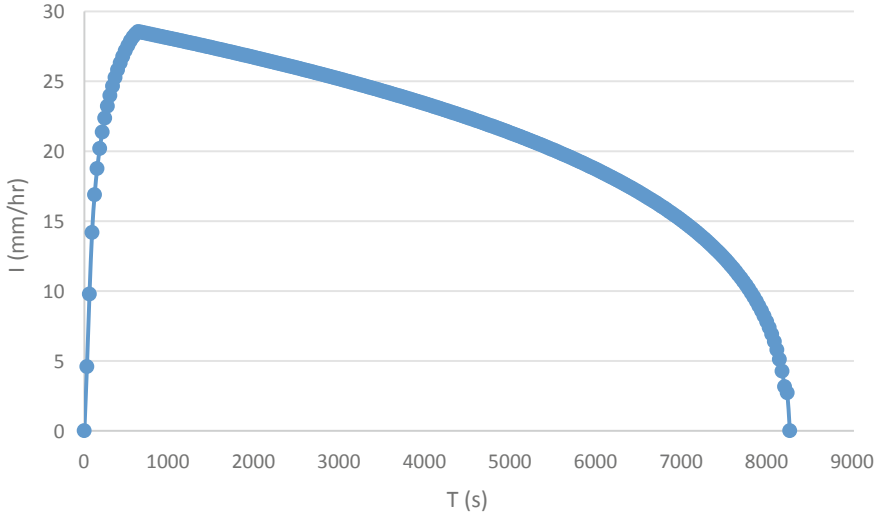


**Fig. 10.10** The simulated rainstorm hyetograph

In Fig. 10.9, the water level variation in the second tank of the device is shown. After the discharge duration of the first tank (700 s), as shown in Fig. 10.5, the water head in the second tank reaches a peak, and after 8000 s, the second tank is completely discharged. This discharge duration is a function of the diameter of the outlet holes of the second tank. By changing this diameter, the intensity and duration of a rainstorm can be determined.

The reviewed reports and studies show an increasing number of flash floods, especially in arid and semiarid zones. A sensitivity analysis of the influencing factors of flash floods shows that the temporal distribution of rainstorms are one of the key factors affecting the occurrence of flash floods. The temporal distributions of rainstorms is the second key factor in characterizing flash floods after antecedent moisture conditions (Lázaro et al. 2014). Zhai et al. (2018) reported that the influences of both soil moisture and the temporal patterns of rainfall on flash floods have not been adequately studied thus far (Zhai et al. 2018). Figure 10.10 shows the temporal patterns of the rainstorm intensity simulated by the device. In this figure, the rainstorm intensities in millimeters per hour and the time in seconds are shown in the vertical axis and the horizontal axis, respectively. As shown in Fig. 10.10, the simulated rainstorm intensity reached its peak as the water head in the second tank reached its peak, and finally, the rainfall intensity reached zero as the second tank fully emptied. By adjusting the valve of the device, various temporal rainstorm patterns can be produced by the device, and the numerical model obtained in this research can be used to find the proper adjustment of the valve for producing rainstorms with a certain temporal pattern for flash flood studies.

## 10.4 Conclusions

Flash flood studies require a new device to expand previous experimental and field studies on the impacts of the various temporal patterns of rainstorms on flash flood characteristics. Current simulation devices can simulate constant-intensity precipitation well; nonetheless, reported studies show the need for more studies on the effects of temporal variations in rainstorms in producing flash floods. In this research, a rainfall hyetograph-generating device is designed and examined based on drop-generating and cascading tanks to produce various rainfall hyetographs for more accurate simulations of rainstorms with different temporal variations. Accordingly, by placing two cascading reservoirs and using reservoir routing in the cascading tanks, a simulator was designed and constructed that could generate hyetographs. Then, the device was calibrated based on observed data. The results of the precipitation values generated with this device showed that it is possible to simulate rainstorms with varied intensities over time as well as produce different hyetographs in terms of the duration to the peak and the rainstorm duration with an accuracy of 95%. Consequently, this device can simulate rainstorms more accurately and can be used to obtain more accurate tests in flash flood studies.

## References

Al-Rawas GA, Valeo C (2009) Characteristics of rainstorm temporal distributions in arid mountainous and coastal regions. J Hydrol 376:318–326

Almutairi NB, Zribi M (2006) Sliding mode control of coupled tanks. Mechatronics 16:427–441

Aminyavari S, Saghafian B, Sharifi E (2019) Assessment of precipitation estimation from the NWP models and satellite products for the spring 2019 severe floods in Iran. Remote Sens 11:2741

Aoki AM, Sereno R (2006) Evaluación de la infiltración como indicador de calidad de suelo mediante un microsimulador de lluvias. Agriscientia 23

Banihabib ME, Tanhapour M (2020) An empirical equation to determine the threshold for rainfall-induced landslides developing to debris flows. Landslides

Cornelis WM, Erpul G, Gabriels D (2004) The ICE wind tunnel for wind and water interaction research. Wind Rain Interact Erosion 195–224

Corona R, Wilson T, D'Adderio LP, Porcù F, Montaldo N, Albertson J (2013) On the estimation of surface runoff through a new plot scale rainfall simulator in Sardinia. Italy Procedia Environ Sci 19:875–884

de Vries AJ, Tyrlis E, Edry D, Krichak S, Steil B, Lelieveld J (2013) Extreme precipitation events in the middle east: dynamics of the active red sea trough. J Geophys Res Atmos 118:7087–7108

Esteves M, Planchon O, Lapetite JM, Silvera N, Cadet P (2000) The 'EMIRE'large rainfall simulator: design and field testing. Earth Surf Process Landforms: J Br Geomorphol Res Group 25:681–690

Fernández-Gálvez J, Barahona E, Mingorance M (2008) Measurement of infiltration in small field plots by a portable rainfall simulator: application to trace-element mobility. Water Air Soil Pollution 191:257–264

Foster I, Fullen M, Brandsma R, Chapman A (2000) Drip-screen rainfall simulators for hydro-and pedo-geomorphological research: the Coventry experience. Earth Surf Process Landforms: J Br Geomorphol Res Group 25:691–707

Grierson I, Oades J (1977) A rainfall simulator for field studies of run-off and soil erosion. J Agric Eng Res 22:37–44

Huang J, Wu P, Zhao X (2013) Effects of rainfall intensity, underlying surface and slope gradient on soil infiltration under simulated rainfall experiments. Catena 104:93–102

Lázaro JM, Navarro JAS, Gil AG, Romero VE (2014) Sensitivity analysis of main variables present in flash flood processes application in two spanish catchments: Arás and Aguilón. Environ Earth Sci 71:2925–2939

Mays L (2001) General characteristics of arid and semiarid regions. Urban drainage in arid and semiarid regions

Moore ID, Hirschi MC, Barfield BJ (1983) Kentucky rainfall simulator. Trans ASAE 26:1085–1089

Mustafa AM, Muhammed H, Szydłowski M (2019) Extreme rainfalls as a cause of urban flash floods; a case study of the Erbil-Kurdistan region of Iraq. Acta Scientiarum Polonorum Formatio Circumiectus 18:113–132

Roughani M, Ghafouri M, Tabatabaei M (2007) An innovative methodology for the prioritization of sub-catchments for flood control. Int J Appl Earth Obs Geoinf 9:79–87

Sangüesa C, Arumí J, Pizarro R, Link O (2010) A rainfall simulator for the in situ study of superficial runoff and soil erosion. Chilean J Agric Res 70:178–182

Tabari H, Willems P (2016) Daily precipitation extremes in Iran: decadal anomalies and possible drivers. JAWRA J Am Water Resour Assoc 52:541–559

Zhai X, Guo L, Liu R, Zhang Y (2018) Rainfall threshold determination for flash flood warning in mountainous catchments with consideration of antecedent soil moisture and rainfall pattern. Nat Hazards 94:605–625